Dislocation network in additive manufactured steel breaks strength–ductility trade-off

Liu, Leifeng; Ding, Qingqing; Zhong, Yuan; Zou, Ji; Wu, Jing; Chiu, Yu-Lung; Li, Jixue; Zhang, Ze; Yu, Qian; Shen, Zhijian

DOI:
10.1016/j.mattod.2017.11.004

Dislocation network in additive manufactured steel breaks strength-ductility trade-off

Leifeng Liu[1#], Qingqing Ding[2#], Yuan Zhong[1], Ji Zou[3], Jing Wu[3], Yu-Lung Chiu[3], Jixue Li[2], Ze Zhang[2], Qian Yu[2*], Zhijian Shen[1*]

1. Department of Materials and Environmental Chemistry, Arrhenius Laboratory, Stockholm University, 10691 Stockholm, Sweden

2. Department of Materials Science & Engineering, Center of Electron Microscopy and State Key Laboratory of Silicon Materials, Zhejiang University, Hangzhou 310027, China

3. School of Metallurgy and Materials, University of Birmingham, B15 2TT, UK

# These authors contributed equally to this work

* E-mail: yu_qian@zju.edu.cn; zhijian.james.shen@mmk.su.se;

Abstract

Most mechanisms used for strengthening crystalline materials, e.g. introducing crystalline interfaces, lead to the reduction of ductility. An additive manufacturing process – selective laser melting breaks this trade-off by introducing dislocation network, which produces a stainless steel with both significantly enhanced strength and ductility. Systematic electron microscopy characterization reveals that the pre-existing dislocation network, which maintains its configuration during the entire plastic deformation, is an ideal "modulator" that is able to slow down but not entirely block the dislocation motion. It also promotes the formation of high density of nano-twins during the plastic deformation. Meanwhile, notable strain rate hardening also contributes to stabilize the plastic deformation. This finding paves the way for developing high performance metals by tailoring the microstructure through additive manufacturing processes.

Key words: Additive manufacturing; Selective laser melting; Stainless steel; Mechanical property; Transmission electron microscopy;

1. Introduction

The motion of dislocations governs the plastic deformation hence the mechanical properties of many metals.[1,2,3] The strength of the metals can be improved by hindering dislocation motion through the designing of microstructure including introducing secondary phases, grain boundaries and other internal interfaces.[4] Unfortunately most of such strategies that effectively strengthen materials sacrifice ductility, resulting in the so called strength-ductility trade-off.[5] Although a few methods have shown the capability of improving strength while retaining the ductility of materials (for instance by introducing coherent twin boundaries[2,6], introducing bimodel grain sizes[7] and by controlling the size, morphology and distribution of secondary phases[8,9]), making final parts with complex shapes from these methods requires intensive additional machining and may even not be feasible in some cases.

Selective laser melting (SLM) is a type of additive manufacturing (AM) processes which is now rapidly changing the ecosystem of manufacturing by enabling the manufacturing of complex components directly from digital files, thus benefiting the customized production and the freedom of designing.[10] During SLM, particle granules are fused directly into 3D components by repetitive scanning of a high energy laser beam over each layer of powder granules, thereby consolidating them via partial or full melting. Another important feature of AM is the ultrafast cooling rate (10^3-10^8 K/s). Unlike the other rapid cooling techniques e.g. splat quenching and melt spinning which can produce only metals in low dimensional shapes e.g. metal powder, ribbon and foil, AM can produce metals in 3-dimensional shapes (bulk parts) with extraordinary high cooling rate.[11-14] The bulk metal parts show microstructures distinct from those produced by traditional manufacturing routes such as casting and wrought processes.[15-21] In this study, we show that a dislocation network structure with the accompanying segregation of the alloying elements produced during SLM manufacturing of 316L stainless steel (316LSS) leads to unprecedented mechanical properties of a combination of enhanced yield strength and ductility compared to those with the same composition but produced in the other manufacturing processes.[22–28] In-situ SEM and TEM study reveals that the dislocation network with the accompanying segregation provides high density of "flexible interfaces" that significantly tunes the dislocation behaviours, resulting in the ameliorated mechanical properties. The results indicate the possibility to directly manufacture products with good combination of strength and ductility while retain the benefits of the process in manufacturing parts with complex or customized geometries.

2. Materials and Methods

2.1 Sample manufacturing process

As received gas-atomized spherical 316LSS powder with the granular size ranging from 10 to 45 µm was purchased from Carpenter powder products AB, Torshälla, Sweden. The standard build was performed by a selective laser melting facility EOSINT M270 (EOS GmbH, Krailling, Germany) equipped with a continuous Nd:YAG fiber laser generator with maximum 200 W power output and typically 70 µm diameter laser spot. During the building process, a layer of powder (20 µm in thickness) was laid by a recoating blade on a steel building plate which was preheated to 80 ^{o}C. The full laser power of 200 W was used and the laser beam was moving at the speed of 850 mm/s. The laser scanned line by line along the same direction at the same layer and with the line spacing of 100 µm. After the scanning was complete, a new layer of powder was laid and the laser scanned the new layer with the scanning direction rotated by 67^{o}. The sample was built up by repeating this process.

To investigate the effect of scanning speed on dislocation cell size, the samples were built up by using standard parameters and the last layer of each sample was scanned by laser with different scanning speed and line spacing (7000 mm/s, 10 µm; 4250 mm/s, 20 µm; 283 mm/s, 300 µm). The SEM images were taken from the area within the top layers.

2.2 Tensile tests

Tensile test specimens (as-build size Φ8 × 52 mm) were prepared by SLM using standard building parameters and machined to cylindrical test specimens (Gage length: 12 mm; gage diameter: 3 mm). All the tensile test bars were built in the same build and with the longitudinal axes along the building direction. Tensile tests were performed according to

ASTM E8 with a strain rate of 0.015 min^{-1} up to yield point, and afterward 0.05 min^{-1} till failure. An extensometer was used to measure the elongation. The reported values in this study for tensile properties were the average values of 5 tests.

2.3 Micropillar tests

For the micropillar compression test, two pellets were cut from the same bar built with the longitudinal axis along the building direction. One of them were packed in the stainless steel envelop and heated to 1050 ^{o}C with the ramp rate of 10 ^{o}C/min, kept for 2 hours and followed by water quench. The other one was kept in the as-SLMed state. Two pellets were grinded and polished before micropillar experiment. A commercial Hysitron PI85 PicoIndenter installed inside a Tescan Mira-3 scanning electron microscope was used for micropillar compressions. The micropillars with dimensions of about 5 µm, length of about 10 µm and tapering angles less than 5 degree were fabricated in a FEI Quanta 3D FEG Focus Ion Beam (FIB) by Ga^{+} ion beam with the current ranging from 30 nA to 0.1 nA at 30 kV. Both of the two micropillars were fabricated from the grains with the (056) plane parallel to the top surface. The micropillars were then compressed using a flat punch diamond tip with diameter of 20 µm with constant loading rate of 100 µN/s^{-1}.

2.4 TEM analysis

TEM specimen were twin-jet electropolished in an alcoholic solution containing 5 vol.% perchloric acid at 30 mA and -25 °C. Equipped with both bright field and annular dark field detectors, a Cs-corrected FEI 80-200 G^2 with Super-X operated at 200 kV is employed to analyse the microstructure and elemental distribution of the SLMed 316LSS. The in-situ tensile tests were achieved by a Gatan model 654 single-tilt straining holder in a FEI Tecnai G2 F20 TEM operated at 200 kV.

SEM images were taken on the etched surfaces. Etching was done by submerging the mechanical polished samples into the etching agent (HF:HNO3:H2O = 1:4:45) for 60 seconds.

3. Results and discussion

3.1 Tensile properties of the SLMed 316LSS and TEM characterization of the dislocation network structure

Fig. 1b shows a component with the dimensions of 28 cm × 16 cm × 16 cm and a built-in complex internal cooling channel system manufactured by using SLM process from 316LSS powders (particle size: 10μm - 45μm) for the potential application as the first wall panel part in the International Thermonuclear Experimental Reactor (ITER). Tensile tests reveal that the SLMed 316LSS shows notable improvement in both strength and ductility compared to the fully dense 316LSS processed by the other manufacturing methods (Fig. 1a).[22–28] The tensile yield strength of 552 ± 4 MPa and elongation to failure of 83.2 ± 0.7 %, was obtained for the SLMed 316LSS (along the building direction). In contrast, the wrought-annealed 316LSS with average grain size of 17.5 μm from Ref.22 shows yield Strength of 244 MPa and failure elongation of 63%.[22] A number of previous research on SLMed 316L reported that the process improves the yield strength but reduces or has little effect on ductility.[11,29,30] The ductility of metals is sensitive to the defects like voids and cracks whose presence largely depends on the process parameters. Only when the defects are supressed, the contribution from the other factors would be revealed.

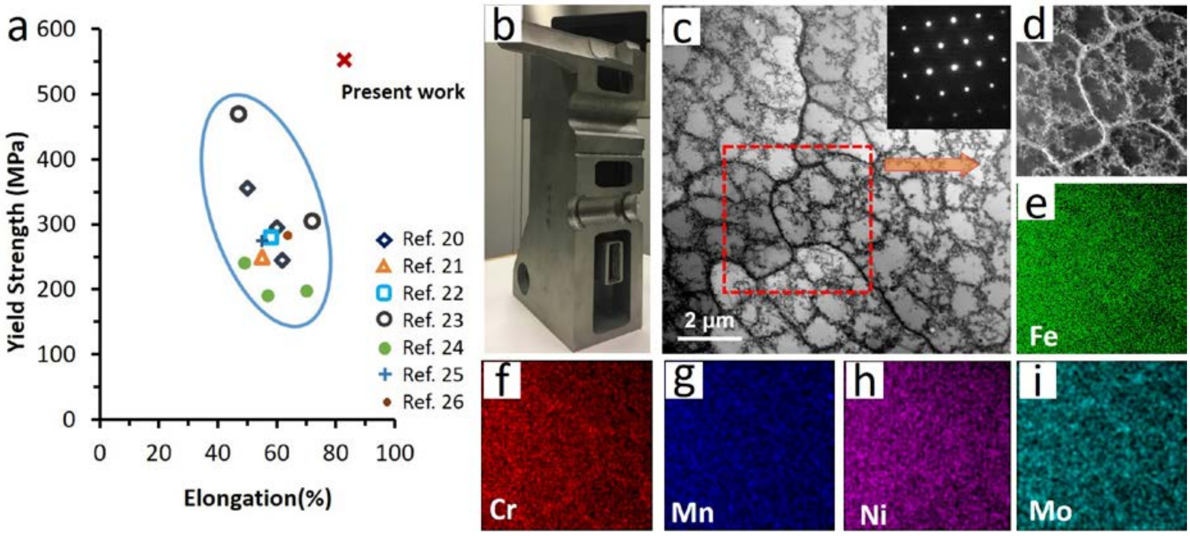

Figure 1. The dislocation network with the accompanying segregation of the alloying elements in SLMed 316LSS. a, The yield strength and ductility data of the SLMed 316LSS and the fully dense 316LSS from literature. The elongation to failure was used. **b**, A photo of the ITER first wall penal part manufactured by SLM. **c**, A bright field (BF) STEM image of the dislocation network in the SLMed 316LSS with the corresponding selected area electron diffraction (SAED) pattern which shows the single grain signal. **d-i**, An annular dark field (ADF) STEM image and elemental distribution maps of the selected area in **c.**

Residual stress can be generated during SLM process, but it was not considered as the main factor affecting the tensile results in this work. Previous studies show that residual stress in SLMed sample can be comparable to the yield strength of the material near the top surface but is much lower in the lower part of the sample.[31-33] The gage section of the tensile test bar in this study is far below the top surface. Moreover the building plate was preheated to 80 ^{o}C during process to reduce the residual stress. Thus the residual stress is unlikely to have much effect on the tensile results. The microstructure of the material is then considered as the main reason for the ameliorated mechanical properties. The SLMed 316LSS is composed of mainly columnar grains with the diameters ranging from a few to tens of micrometres and lengths up to hundreds of micrometres. TEM analysis reveals a unique dislocation network embedded in individual grains. The dislocation network has been previously found only in 1D or 2D structures (e.g. the welding track or laser treated metal surface[34,35]), but not in bulk metals produced by any other manufacturing methods. Figure 1c shows the typical dislocation network within a coarse grain, with dislocations concentrated as the wall of columnar cells. SEM analysis shows that the cells have an average diameter of around 500 nm and lengths ranging from a few micrometres to a few tens micrometres. The dislocation cells are often aligned with the temperature gradient direction in the solidification process. The elemental maps (Fig. 1e-i) from energy dispersive spectroscopy (EDS) analysis show that the element distribution on the dislocation network is fairly uniform with slight segregation of Cr, Mo and Mn at the walls. Quantitative EDS analysis was performed on five random spots at the dislocation walls and in the other areas, respectively. The results (Table 1) show that Mo, Mn, Cr and Ni content at the dislocation network are all higher than those in the other areas. The formation of dislocation network structure with the accompanying segregation of the alloying elements is due to the cellular growth mode under the high temperature gradient and high growth rate condition.[35] Slight orientation differences for the neighbouring cells cause the dense dislocation walls to form when cells grow together into coarse single grains. Meanwhile, the solidification front rejects the alloying elements to the liquid phase leading to higher content of alloying elements at the later solidified region – the cell boundaries.[36] Dislocation cells can also form after plastic deformation in a wide range of metals. The flow strength of the deformed metal is inversely linked to the size of such cells. Therefore the dislocation cells in SLMed 316LSS is presumably the main reason of the improved mechanical property.

Table 1. The content of the elements at the cell wall and inside the cell (wt.%) from EDS analysis.

Element / position	Fe	Cr	Ni	Mo	Mn
Cell wall	65.9±1.30	18.5±0.65	11.0±0.16	2.8±0.50	1.74±0.06
Cell inner	69.9±0.11	16.7±0.24	10.3±0.14	1.59±0.11	1.42±0.05

3.2 The strengthening effect of dislocation network confirmed by Micropillar compression tests

To examine the role of this characteristic dislocation network in affecting the mechanical properties, we performed micropillar compression tests on two samples, viz. the as-SLMed 316LSS whose microstructure was decorated by dislocation network and SLMed-annealed 316LSS which was free of dislocation network after annealing at 1050 ^{o}C for 2 hours (Fig. 2a, b, d, e).

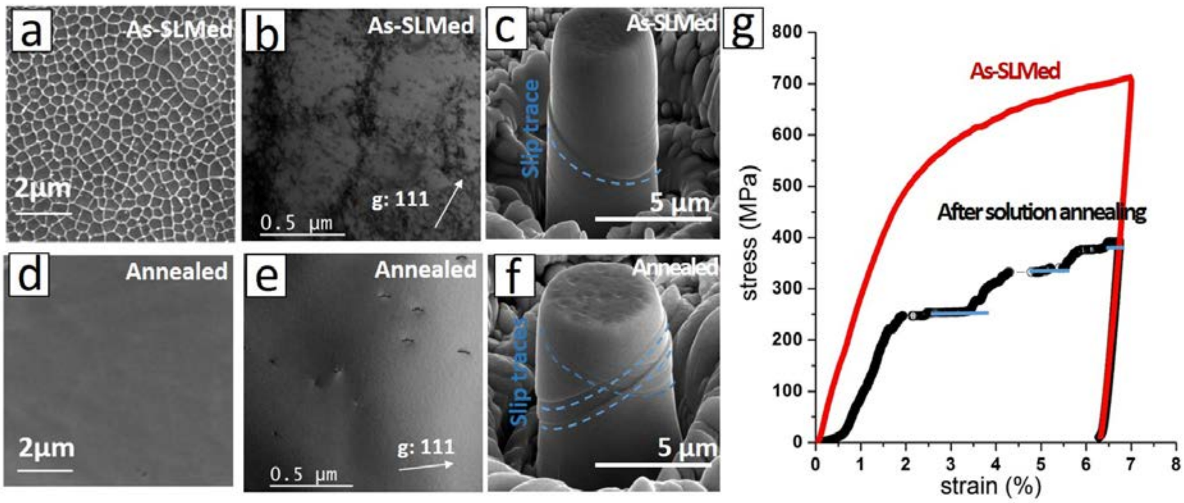

Figure 2. Micropillar compression test result. a, **b**, SEM and TEM images of the microstructure of the as-SLMed 316LSS. **c,** Compression tested micropillar of the as-SLMed 316LSS. **d, e,** SEM and TEM images of the microstructure of the annealed 316LSS. **f,** Compression tested micropillar of the annealed 316LSS. **g**, The engineering stress-strain curves obtained from two micropillars. The as-SLMed sample shows almost doubled yield strength and much smoother plastic flow behavior than the annealed sample.

Both single crystal micropillar samples were of the same size (5 μm in diameter) before pressing and were compressed along the [0 5 6] direction. As shown in Fig. 2g, the yield strength is about 240 MPa for the annealed sample in contrast to 460 MPa for the as-SLMed sample. The three remarkable plateaus on the stress-strain curve correspond to the three slip traces on the surface of the annealed micropillar (Fig. 2f), indicating that catastrophic shear-off happened quite often due to the escape of large number of dislocations from the intersections of the same slip planes and the surface. In contrast, the as-SLMed pillar had smoother plastic flow behaviour. It indicates that with the dislocation network, the as-SLMed pillar had much better ability of dislocation storage where dislocations found significant difficulty during glide before they eventually slipped out from the surface therefore displayed both higher strength and better plastic stability.

3.3 Effects of the dislocation network on dislocation motion and twin formation revealed by in-situ TEM analysis

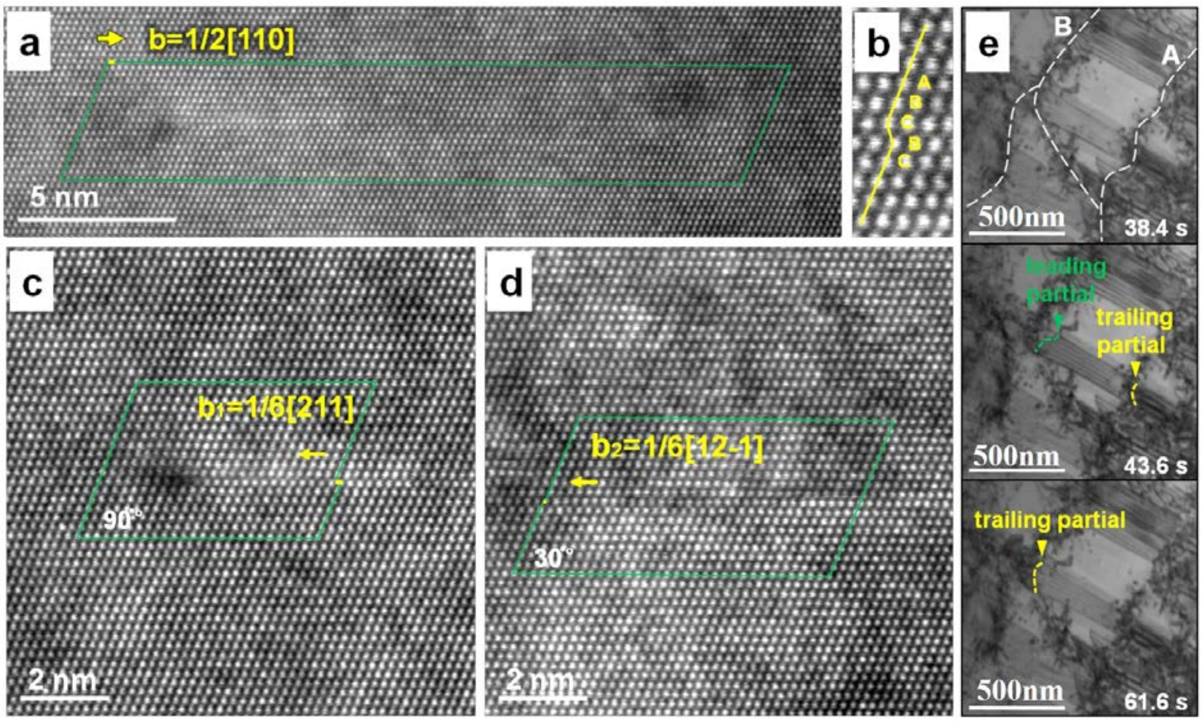

Figure 3. Dislocations in SLMed 316LSS. a, A high-angle annular dark field (HAADF)-STEM image of a partial dislocation pair within a cell in the as-SLMed sample. **b**-**d**, High resolution annular dark field (ADF)-STEM images showing the stacking fault, trailing partial dislocation and leading partial dislocation in (**a**). **e**, Screenshots from the Video 1 showing interaction between partial dislocations and dislocation cell walls.

The details of the dynamic motion and interaction of dislocations within such dislocation network were further investigated by performing in-situ TEM mechanical testing at room temperature by using a Gatan in-situ straining holder. The major carrier for plastic deformation was partial dislocations, whose motion was significantly but not fully impeded by the dislocation network. Dislocations widely dissociated into Shockley partials with jerky motion when they were temporarily trapped by the dislocation walls and would move forward again with the increase of applied stress (Video 1). For instance, as shown in Fig. 3a-d, the partial dislocations within a cell in the as-SLMed sample have Burgers vector 1/6[211] and 1/6[12-1], respectively. The dislocations in the cell walls are also mostly dissociated partial dislocations with Burgers vector 1/6<112>. Figure 3e shows the dynamic evolution of stacking fault, which corresponds to the motion of partial dislocation pairs through the dislocation cells. When the external stress was high enough, a leading partial was emitted from a cell wall “A” and stopped at the cell wall “B” against it. At this moment, the trailing partial was still trapped by the cell wall “A”. As the applied stress increased gradually, the leading partial overcame the impediment of wall “B” and glided into the neighbouring cell. The trailing partial glided to wall “B” as well. Clearly the motion of dislocations in SLMed 316LSS was hindered but not fully stopped by these cell walls. Slip transferred across the cells with increasing strain; therefore the strength was enhanced without sacrificing the ductility. This is a scenario similar to the coherent twin boundaries reported before.[2] Besides the impediment effect, the complex dislocation network with mostly dissociated partial dislocations might also have supplied sites for nucleation of dislocation loops, with which the dislocation interactions became even more prolific and complicated.

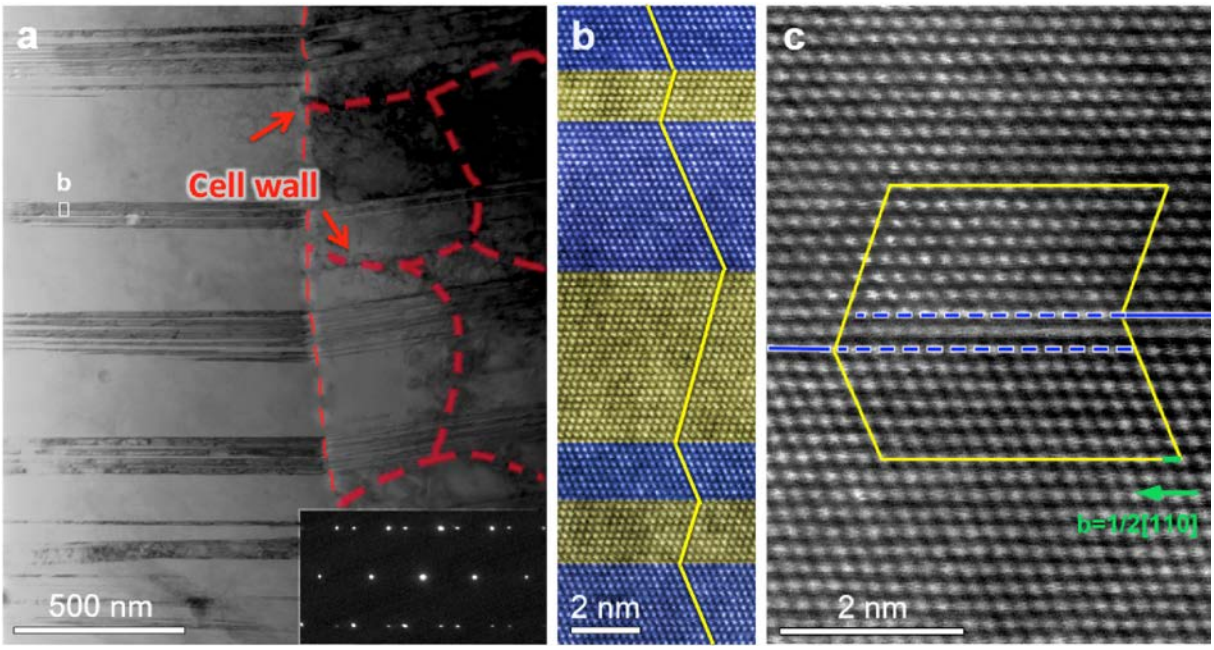

Figure 4. STEM micrographs of the SLMed 316LSS after deformation. a, High density of nano-twins in a BF-STEM image. The inset is the selected area electron diffraction pattern obtained from the left side of the sample in (**a**). **b**, **c**, High resolution (HR)-STEM micrographs showing the atomic structures of the bunched nano-twins and twin boundary with a step. The twin and matrix are colorized into blue and yellow, respectively.

Meanwhile, the cell walls could also trap partial dislocations so that some of the paired dislocations lost their partners. Consequently deformation twinning formed as the same type of partial dislocations glided on the adjacent planes. Figure 4a shows nano-twins formed after deformation. The dislocation network was found in the whole visible region; however, due to the slight orientation difference the network on the left side was less visible under this imaging condition. The slim nano-twins oriented along the same direction and usually propagated through several cells. It was also observed that the nano-twins were bunched and initiated from the cell walls and not necessarily from the grain boundaries. Figure 4b shows a HR-STEM image of the nano-twin structure; the thickness of twins ranged from 2 nm to 6 nm in general. However as shown in Fig. 4c, the stable twin can be as thin as two atomic layers, which supports the layer by layer growth mechanism of twins in this case and it experimentally confirms the theoretical simulation which proposed that the minimum thickness of a stable twin in FCC structure is 2 atomic layers.[34] Those nano-twins should have significant influence on dislocation motion, resulting in stable plastic deformation by strain hardening through the dynamic Hall-Petch effect similar to that in nano-twined copper and TWIP steels.[38, 39]

3.4 The mechanism of simultaneously improvements of strength and ductility

Combining the multiscale mechanical properties-structure characterizations and in-situ TEM testing, it is confirmed that the pre-existing dislocation network structure has significant contribution to the high strength and ductility of as-SLMed 316LSS. Firstly the pre-existing dislocation network impedes dislocation motion and thus increases dislocation storage contributing as the main mechanism to the high yield strength. Meanwhile, the segregated alloying elements at the cell walls provide an extra solid solution strengthening effect. Secondly, with the increase of stress, the impeded dislocations are allowed to transmit through the dislocation walls; meanwhile the pinning effect from the segregated atoms effectively stabilizes the dislocation network to maintain its size during the entire plastic deformation, enabling the stable plastic flow. In addition, the misorientation between cells can also contribute to the stability of the dislocation network as well as provides dislocation sources for the continuous plastic flow. Dislocation cells can also form in a wide range of metals after moderate to large strain. In contrast, such dislocation cells strengthen deformed metals but reduce the tensile elongation. A major difference from the cells formed in SLM is that the wall of such dislocation cells is mobile and the cells shrink as the increase of the stress. The good stability of pre-existing dislocation network structure even at ultra-high stress level in our as-SLMed 316LSS is crucial for the enhancement of ductility.

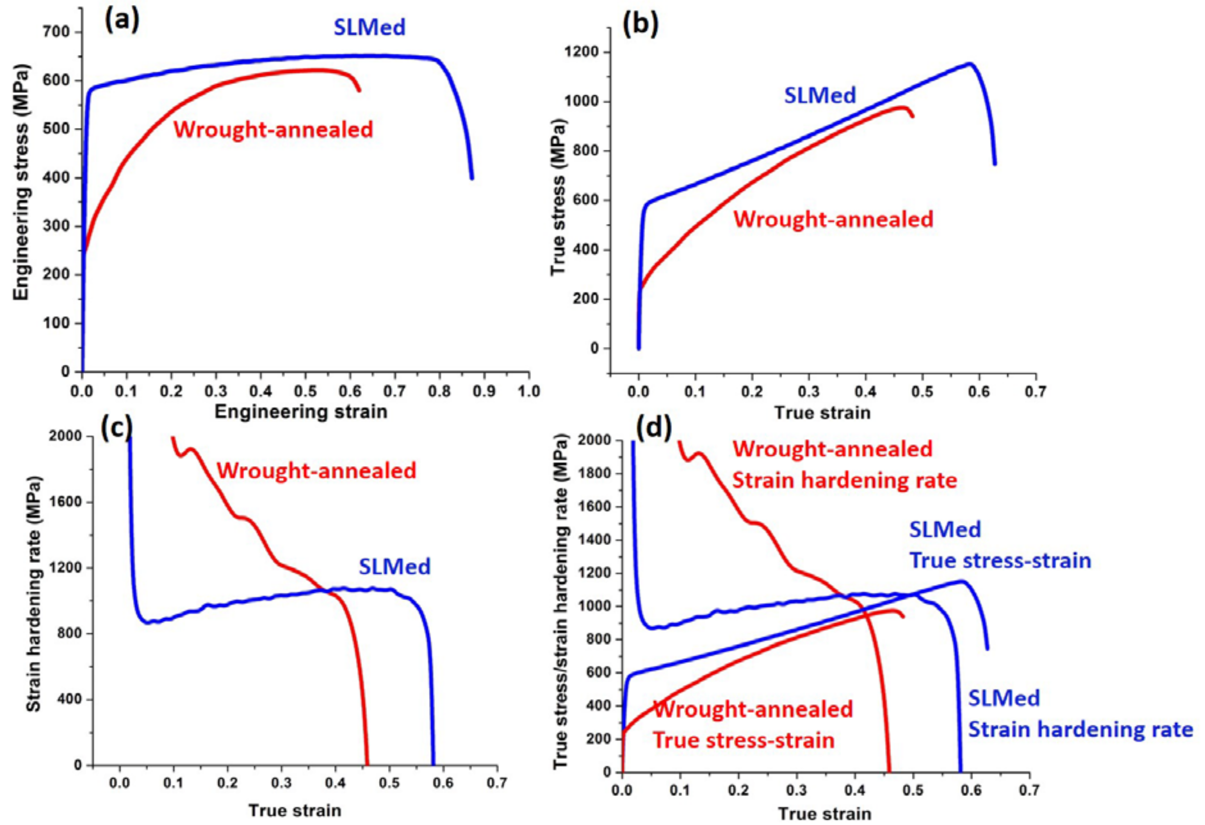

Figure 5. Tensile properties of the SLMed 316LSS from the present work and the wrought-annealed 316LSS with average grain size of 17.5 µm from Ref. 22. a, Engineering tensile stress-strain curves. **b**, True stress-strain curves. **c,** Strain hardening rate curves. **d,** Comparison of the strain hardening rate and true stress of both SLMed and wrought-annealed 316LSS. Bar specimens with gage diameter and length of 3 mm and 12 mm were used for tensile test of SLMed samples. Plate specimens with gage dimensions of 12.5 × 57 × 0.75 mm was used in Ref. 22 for the tensile test of wrought-annealed samples.

In general the increase of ductility is achieved by delaying the onset of necking. The necking caused by plastic instability takes place when the Hart criterion is satisfied ($\frac{\mathrm{d}\sigma}{\mathrm{d}\varepsilon} + m \cdot \sigma \leq \sigma$, where σ is the true stress, ε is the true strain and m is the strain rate sensitivity). So both the strain hardening ($\frac{\mathrm{d}\sigma}{\mathrm{d}\varepsilon}$) and strain rate hardening ($m \cdot \sigma$) contribute to the delay of necking.[37] In wrought-annealed 316LSS, the contribution from strain rate hardening is not significant due to a negligible m value at the latter stage of plastic deformation.[28] In contrast, SLMed 316LSS shows notable elongation after the flow stress outweigh the strain hardening rate, which is presumably from the contribution of strain rate hardening (Fig. 5d). Similar to the ultrafine and nanocrystalline Ni,[41] the concentrated dislocations in dislocation walls lead to a small activation volume and hence a high m value. Besides nano-twins formed during deformation can also cause the increase of m value. On the other hand, the evolution of strain hardening rate also plays an important role for the high tensile elongation of SLMed 316LSS. The strain hardening rate of SLMed 316LSS starts at a low value but maintains stable and even gradually increases during entire plastic deformation till the failure. While the wrought-annealed 316LSS shows initially high strain hardening rate but with substantial decrease afterward (Fig. 5c). The difference in the strain hardening rate is highly related to the distinct microstructural evolution processes in the two 316L stainless steels due to the different stability of the dislocation cellular structure. In SLMed 316L, the pre-existing dislocation network structure formed during manufacturing is pinned by the elements segregation and the misorientation across the cell walls. The characteristic size of the dislocation network structure is retained even at the late stage of the plastic deformation when high flow stress is reached. The misorientation across the cell walls can also act as dislocation source. These enable continues dislocation motion, nanotwins formation and thus the stable plastic flow during the entire plastic deformation. Meanwhile the formation of nano-twins promoted by the dislocation network also contributes to the strain hardening through dynamic Hall-Petch effect to delay the necking. On the contrary, in wrought-annealed 316LSS, dislocation network structure forms during plastic deformation, which contributes to strain hardening rate in the beginning. However, the cells later shrink to small sizes and the dynamic recovery at cell boundaries leads to the decrease of work hardening rate. [42-44]

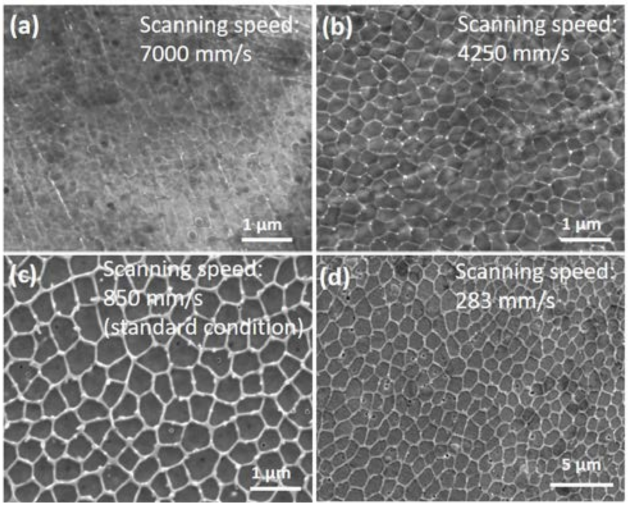

Figure 6. Different scanning speeds result in different sizes of the dislocation cells. a-d, SEM images from the etched surfaces of the samples built with laser scanning speed of (**a**) 7000 mm/s; (**b**), 4250 mm/s; (**c**) 850 mm/s and (**d**) 283 mm/s.

Importantly the cell size and morphology of the dislocation network which are sensitive to the cooling rate and temperature gradient are also tunable by changing the cooling speed. As shown in Fig. 6, the cell size of the dislocation network is effectively adjusted to be around 200 nm, 250 nm, 500 nm and 1 µm, respectively, by using different scanning speed (7000, 4250, 850 and 283 mm/s) to tune the cooling speed. It indicates that the mechanical properties of SLMed alloys can be designed purposefully based on its controllable microstructure-properties relationship.

4. Conclusions

To sum, besides the ability to produce complex shaped parts, the AM processes also provide ultra-fast cooling rate during solidification which results in unique microstructure that consequently leads to outstanding mechanical properties in bulk metal parts that is not possible to be achieved by any other so far established manufacturing method. A systematic SEM and TEM work reveals that the dislocation network with the accompanying segregation of alloying elements acts as stable and “soft” barriers that hinder dislocation motion for strength but meanwhile guarantee continuous plastic flow by allowing dislocations from transmitting. This strategy to improve both the strength and ductility by introducing a dislocation network may also be applied to other alloys with low stacking fault energy. In addition, the mechanical properties can potentially be designed purposefully since its microstructure is directly tuneable by scanning parameters. This work paves the way for developing high performance metals with desired mechanical properties by in situ tailoring the microstructure during the manufacturing process thus further boosting the AM as a disruptive technology to reshape the manufacturing.

Acknowledgements

Thanks to Dr. Mirva Erikson and Jon Olsen for the proof reading.

This work is financially supported by Fusion for Energy (F4E) [F4E-GRT-516]; Chinese 1000-Youth-Talent Plan [Qian Yu]; 111 project [No.B16042]; National Natural Science Foundation of China [51671168]; and the State Key Program for Basic Research in China [No. 2015CB65930].

Reference

1. W.F. Smith, & J. Hashemi, Foundations of materials science and engineering, McGraw-Hill, New York, 2005.
2. D. Hull, D.J. Bacon, Introduction to Dislocations, fourth ed., Elsevier, Amsterdam, 2001.
3. Q. Yu, et al. Origin of dramatic oxygen solute strengthening effect in titanium, Science 347 (2015) 635–639.
4. K. Lu, L. Lu, S. Suresh, Strengthening materials by engineering coherent internal boundaries at the nanoscale, Science 324 (2009) 349–652.
5. K. Kumar, H. Van Swygenhoven, S. Suresh, Mechanical behavior of nanocrystalline metals and alloys, Acta Mater. 51 (2003) 5743–5774.
6. L. Lu, Y. Shen, X. Chen, L. Qian, K. Lu, Ultrahigh strength and high electrical conductivity in copper, Science 304 (2004) 422–426.
7. Y. Wang, M. Chen, F. Zhou, E. Ma, High tensile ductility in a nanostructured metal, Nature 419 (2002) 912–915.
8. X. Wu, et al. Heterogeneous lamella structure unites ultrafine-grain strength with coarse-grain ductility, Proc. Natl. Acad. Sci. 112 (2015) 14501–14505.
9. S. H. Kim, H. Kim, N.J. Kim, Brittle intermetallic compound makes ultrastrong low-density steel with large ductility, Nature 518 (2015) 77–79.
10. B. Berman, 3-D printing: The new industrial revolution, Bus. Horiz. 55 (2012) 155–162.
11. D. Herzog, V. Seyda, E. Wycisk, C. Emmelmann, Additive manufacturing of metals, Acta Mater. 117 (2016) 371–392.

12. S.A. Khairallah, A.T. Anderson, A. Rubenchik, W. King, Laser powder-bed fusion additive manufacturing: Physics of complex melt flow and formation mechanisms of pores, spatter, and denudation zones, Acta Mater. 108 (2016) 36–45.

13. E. W. CollingsA. J. MarkworthJ. K. McCoyJ. H. Saunders, Splat-quench solidification of freely falling liquid-metal drops by impact on a planar substrate, J. Mater. Sci. 25 (1990) 3677-3682.

14. D. Pavuna, Production of metallic glass ribbons by the chill-block melt-spinning technique in stabilized laboratory conditions, J. Mater. Sci. 16 (1981) 2419-2433.

15. X.P. Li, et al. A selective laser melting and solution heat treatment refined Al-12Si alloy with a controllable ultrafine eutectic microstructure and 25% tensile ductility, Acta Mater. 95 (2015) 74–82.

16. B. Qian, et al. Defects-tolerant Co-Cr-Mo dental alloys prepared by selective laser melting, Dent. Mater. 31 (2015) 1435–1444.

17. G. A. Ravi, C. Qiu, M.M. Attallah, Microstructural control in a Ti-based alloy by changing laser processing mode and power during direct laser deposition, Mater. Lett. 179 (2016) 104–108.

18. L. Thijs, F. Verhaeghe, T. Craeghs, J.V. Humbeeck, J.P. Kruth, A study of the microstructural evolution during selective laser melting of Ti–6Al–4V, Acta Mater. 58 (2010) 3303–3312.

19. B. Vrancken, L. Thijs, J.P. Kruth, J.V. Humbeeck, Microstructure and mechanical properties of a novel β titanium metallic composite by selective laser melting, Acta Mater. 68 (2014) 150–158.

20. J. Wu, X.Q. Wang, W. Wang, M.M. Attallah, M.H. Loretto, Microstructure and strength of selectively laser melted AlSi10Mg, Acta Mater. 117 (2016) 311–320.

21. Y. Zhong, L. Liu, S. Wikman, D. Cui, Z. Shen, Intragranular cellular segregation network structure strengthening 316L stainless steel prepared by selective laser melting. J. Nucl. Mater. 470 (2016) 170–178.

22. W.A. Poling, Grain Size Effects in Micro-Tensile Testing of Austenitic Stainless Steel, MS thesis, Colorado School of Mines, 2012.

23. X.H. Chen, J. Lu, L. Lu, K. Lu, Tensile properties of a nanocrystalline 316L austenitic stainless steel, Scr. Mater. 52 (2005) 1039–1044.

24. S. Maloy, et al. The mechanical properties of 316L/304L stainless steels, Alloy 718 and Mod 9Cr–1Mo after irradiation in a spallation environment, J. Nucl. Mater. 296 (2001) 119–128.

25. F.K. Yan, G.Z. Liu, N.R. Tao, K. Lu, Strength and ductility of 316L austenitic stainless steel strengthened by nano-scale twin bundles, Acta Mater. 60 (2012) 1059–1071.

26. A.M. Brass, J. Chêne, Hydrogen uptake in 316L stainless steel: Consequences on the tensile properties, Corros. Sci. 48 (2006) 3222–3242.

27. V. Ganesan, M.D. Mathew, K.B. Sankara Rao, Influence of nitrogen on tensile properties of 316LN SS, Mater. Sci. Technol. 25 (2009) 614–618.

28. G.S. Langdon, G.K. Schleyer, Unusual strain rate sensitive behaviour of AISI 316L austenitic stainless steel, J. Strain Analysis 39 (2015) 71-86.

29. H.D. Carlton, A. Haboub, G.F. Gallegos, D.Y. Parkinson, A.A. MacDowell, Damage evolution and failure mechanisms in additively manufactured stainless steel, Mater. Sci. Eng. A 651 (2016) 406-414.

30. A. Riemer, S. Leuders, M. Thöne, H.A. Richard, T. Tröster, T. Niendorf, On the fatigue crack growth behavior in 316L stainless steel manufactured by selective laser melting, Eng. Fract. Mech. 120 (2014) 15-25.

31 X. Song, et al, Residual stresses and microstructure in Powder Bed Direct Laser Deposition (PB DLD) samples, Int. J. Mater. Form. 8 (2015) 245–254.

32 M.Shiomi, K.Osakada, K.Nakamura, T.Yamashita, F.Abe, Residual Stress within Metallic Model Made by Selective Laser Melting Process, CIRP Annals, 53 (2004) 195-198.

33. I.A. Roberts, Investigation of residual stresses in the laser melting of metal powders in

additive layer manufacturing, PhD Thesis, University of Wolverhampton, 2012.

34. V. Shankar, T.P. Gill, S. Mannan, S. Sundaresan, Effect of nitrogen addition on microstructure and fusion zone cracking in type 316L stainless steel weld metals, Mater. Sci. Eng. A 343 (2003) 170–181.

35. S. Kou, Welding metallurgy, John Wiley & Sons, New Jersey, 2003.

36. E. Kannatey-Asibu, Principles of laser materials processing, John Wiley & Sons, New Jersey, 2009.

37. S. Ogata, J. Li, S. Yip, Energy landscape of deformation twinning in bcc and fcc metals, Phys. Rev. B 71 (2005) 224102.

38. L. Lu, X. Chen, X. Huang, K. Lu, Revealing the maximum strength in nanotwinned copper, Science 323 (2009) 607–610.

39. Z. Li, K.G. Pradeep, Y. Deng, D. Raabe, C.C. Tasan, Metastable high-entropy dual-phase alloys overcome the strength–ductility trade-off. Nature 534 (2016) 227-230.

40. E.W. Hart, Theory of the tensile test, Acta Metallurgica 15 (1967) 351-355.

41. Y.M. Wang, A.V. Hamza, E. Ma, Temperature-dependent strain rate sensitivity and activation volume of nanocrystaline, Ni. Acta Mater. 54 (2006) 2715-2726.

42. M. Nabil Bassim, R.J. Klassen, Variation in dislocation cell size with local strain in a low alloy steel, Mater. Sci. Eng. 81 (1986) 163–167.

43. R.N. Gardner, T.C. Pollock, H.G.F. Wilsdorf, Crack initiation at dislocation cell boundaries in the ductile fracture of metals, Mater. Sci. Eng. 29 (1977) 169 – 174.

44. X. Feaugas, On the origin of the tensile flow stress in the stainless steel AISI 316L at 300 K: back stress and effective stress, Acta Mater. 47 (1999) 3617–3632.

Author Contributions

Z.S., Q.Y. and L.L. designed the research; Y.Z. and L.L. fabricated the samples; Q.D. performed the in-situ TEM work and the data analysis; J.Z. and J.W. carried out the micropillar compression tests; L.L., Q.D., Q.Y., L.C and Z.S. wrote the manuscript; all the authors contributed to the discussions and commented the manuscript.

Competing Financial Interests statement

The authors declare no competing financial interests.